CHEMISTRY
A European Journal

A Journal of
ChemPubSoc Europe

Accepted Article

Title: Fluorescent and Biocompatible Ruthenium-Coordinated Oligo(p-phenylenevinylene) Nanocatalyst for Transfer Hydrogenation in Mitochondria of Living Cells

Authors: Shu Wang

To be cited as: *Chem. Eur. J.* 10.1002/chem.201905448

Link to VoR: http://dx.doi.org/10.1002/chem.201905448

Supported by
ACES

WILEY-VCH

10.1002/chem.201905448

COMMUNICATION

WILEY-VCH

Fluorescent and Biocompatible Ruthenium-Coordinated Oligo(*p*-phenylenevinylene) Nanocatalyst for Transfer Hydrogenation in Mitochondria of Living Cells

Nan Dai[a,b], Hao Zhao[a,b], Ruilian Qi[a], Yanyan Chen[a], Fengting Lv[a], Libing Liu[a,b] and Shu Wang[a,b]*

Abstract: It is challenging to design metal catalysts for *in situ* transformation of endogenous biomolecules with good performance inside living cells. Herein, we report a multifunctional metal catalyst, ruthenium-coordinated oligo(*p*-phenylenevinylene) (OPV-Ru), for intracellular catalysis of transfer hydrogenation of nicotinamide adenine dinucleotide (NAD^+) to its reduced format (NADH). Owing to its amphiphilic characteristic, OPV-Ru possesses good self-assembly capability in water to form nanoparticles through hydrophobic interaction and π-π stacking, and numerous positive charges on the surface of nanoparticles displayed a strong electrostatic interaction with negatively charged substrate molecules, creating a local microenvironment for enhancing the catalysis efficiency in comparison to dispersed catalytic center molecule (TOF value was enhanced by about 15 folds). OPV-Ru could selectively accumulate in mitochondria of living cells. Benefiting from its inherent fluorescence, the dynamic distribution in cells and uptake behavior of OPV-Ru could be visualized under fluorescence microscopy. This work represents the first demonstration to perform a multifunctional organometallic complex to catalyze natural hydrogenation transformation in specific subcellular compartments of living cells with excellent performance, including fluorescent imaging ability, specific mitochondria targeting, good chemoselectivity and high catalysis efficiency.

Synthetic metal catalysts, as an alternative to natural enzymes, have been broadening the scope of intracellular chemical transformations[1-4]. The design and synthesis of new metal catalysts creates vast possibilities for their application in biosystems, such as developing metal-based drugs, *in situ* synthesizing fluorescent molecules and activating prodrugs[5-7]. However, due to the complexity of cellular environment, the transformation mediated by metal catalysts inside living cells is quite difficult from that in aqueous solution. It requires the metal catalysts to possess many properties including good biocompatibility, stability in physiological conditions, certain water dispersibility as well as hydrophobicity for easy uptake by cells, high activity, etc. Despite of these challenges, numerous metal catalysts have been successfully developed for intracellular catalysis, including metal nanoparticles[8-10], entrapped metal nanoparticles[11] and metal complexes[12-13]. However, fluorescent traceable metal catalysts that can target specific subcellular organelles with good intracellular catalysis ability have been rarely reported. Considering that, it would be appealing to design a fluorescent organelle-targeted metal catalyst for intracellular catalysis.

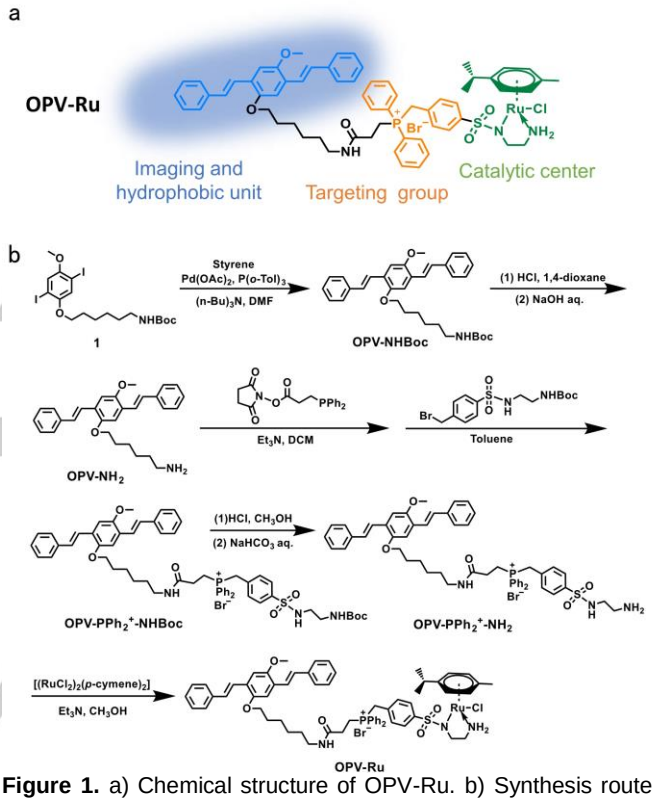

Figure 1. a) Chemical structure of OPV-Ru. b) Synthesis route of OPV-Ru.

As oligo(*p*-phenylenevinylene) (OPV) and its derivatives are easy to assemble in water through π-π stacking and hydrophobic interaction, it will contribute to amplifying the function of functional groups through improving local concentration[14]. Also due to their good biocompatibility, OPV derivatives have been widely applied in biological field such as imaging and cancer therapy[15-16]. In view of this, it is exciting to know whether it is possible to enhance the catalytic activity inside living cells by linking a metal active site to an OPV backbone. In addition, OPV derivatives usually exhibit strong fluorescence under visible light excitation, which will provide advantages for studying the endocytosis mechanism of metal catalyst and its dynamic distribution inside cells. Furthermore, because of its significance in regulating cell functions, mitochondrion was chosen as a certain place for intracellular catalysis. Based on above considerations, herein, we design an oligo(*p*-phenylenevinylene)-ruthenium complex (OPV-Ru), composed of OPV backbone, a mitochondria targeted group and a catalytic activity center (**Fig. 1a**). The activity center is a Noyori-type ruthenium transfer hydrogenation catalyst which could catalyze the hydrogenation of C=O of aldehydes, ketones and C=N of imines[17-19]. Benzyldiphenylphosphonium which is similar to triphenylphosphonium (TPP) is utilized as the targeting

[a] Prof. S. Wang, Dr. L. Liu, Dr. F. Lv, N. Dai, H. Zhao, Dr. R. Qi, Dr. Y. Chen
Beijing National Laboratory for Molecular Sciences, Key Laboratory of Organic Solids, Institute of Chemistry, Chinese Academy of Sciences, Beijing 100190, P. R. China.
E-mail: wangshu@iccas.ac.cn

[b] Prof. S. Wang, Dr. L. Liu, N. Dai, H. Zhao
College of Chemistry, University of Chinese Academy of Sciences, Beijing 100049, P. R. China

Supporting information for this article is given via a link at the end of the document.

10.1002/chem.201905448

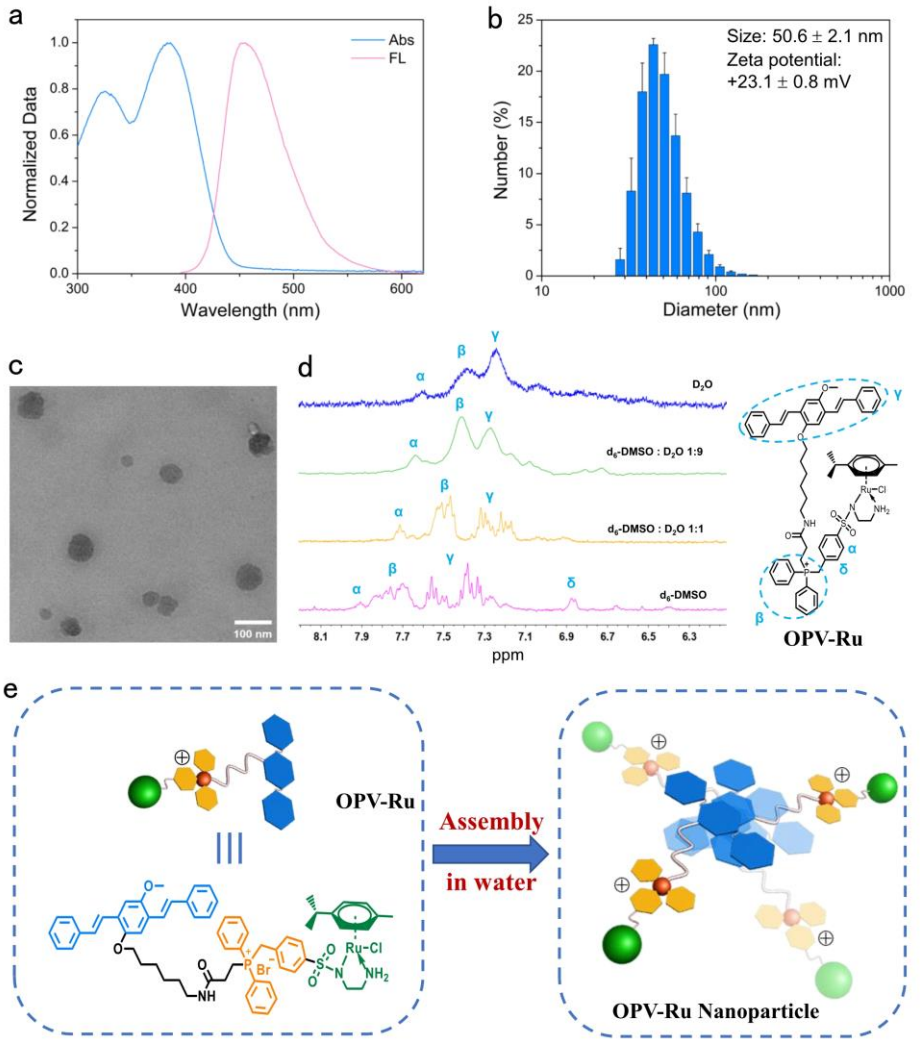

Figure 2. a) Absorption and emission spectra. b) DLS analysis and zeta potential measurement, [OPV-Ru] = 100 μM. c) TEM image, [OPV-Ru] = 100 μM. d) Solvent-dependent ^{1}H NMR spectra, [OPV-Ru] = 200 μM. e) Schematic self-assembly of OPV-Ru in water.

group. TPP cation has been demonstrated numerously to be capable of targeting mitochondria efficiently[20]. It is noted that bioactive molecule nicotinamide adenine dinucleotide (NAD^+) is a crucial coenzyme in eukaryotic cells, which plays a critical role in a variety of physiological activities including cell material metabolism, energy synthesis and cell DNA repair[21-22]. The interconversion between NAD^+ and its reduced format (NADH) regulates many metabolic pathways, including glycolysis, citric acid cycle and oxidative phosphorylation[23-24]. Besides, the NAD^+/NADH ratio is also a symbol of redox state of mammalian cell[25]. We therefore choose this natural transformation of NAD^+ to NADH as a model reaction catalyzed by OPV-Ru.

Fig. 1a shows the chemical structure of OPV-Ru. OPV backbone with three benzene rings and a six-carbon alkyl chain was designed for cell imaging and its hydrophobicity provides driving force for self-assembly in water. Cationic benzyldiphenylphosphonium group and ruthenium complex were covalently linked to the end of the alkyl chain acting for mitochondria targeting and catalysis, respectively. The positive charge ensures a good water dispersibility of the catalyst. In brief, monomer **1** reacted with styrene to get OPV-NHBoc, which was deprotected to OPV-NH_2 afterwards. OPV-NH_2 reacted with the active ester of 3-(diphenylphosphino)propionic acid and then with active benzyl bromide to produce a positively charged OPV-PPh_2^+-NHBoc. After removing the protective group, OPV-PPh_2^+-NH_2 coordinated with ruthenium precursor to generate the target metal complex OPV-Ru (**Fig. 1b**). Detailed synthetic procedures and molecular characterizations are provided in Supporting Information.

The photophysical properties of OPV-Ru were studied in water. As shown in **Fig. 2a**, the OPV-Ru complex exhibits two absorption peaks respectively at 320 nm and 380 nm, and an emission maximum at 450 nm. The absolute fluorescence quantum yield of OPV-Ru was measured to be 6.7% in water. To study the aggregation of OPV-Ru in water, dynamic light scattering (DLS), ^{1}H nuclear magnetic resonance (NMR) spectroscopy and transmission electron microscopy (TEM) were employed. DLS measurement results showed that OPV-Ru formed nanoparticles with an average diameter of 50.6 ± 2.1 nm and its zeta potential was +23.1 ± 0.8 mV (**Fig. 2b**), which also was confirmed by TEM image (**Fig. 2c**). Broad proton signals for aromatic rings of OPV-Ru in water suggested that OPV-Ru

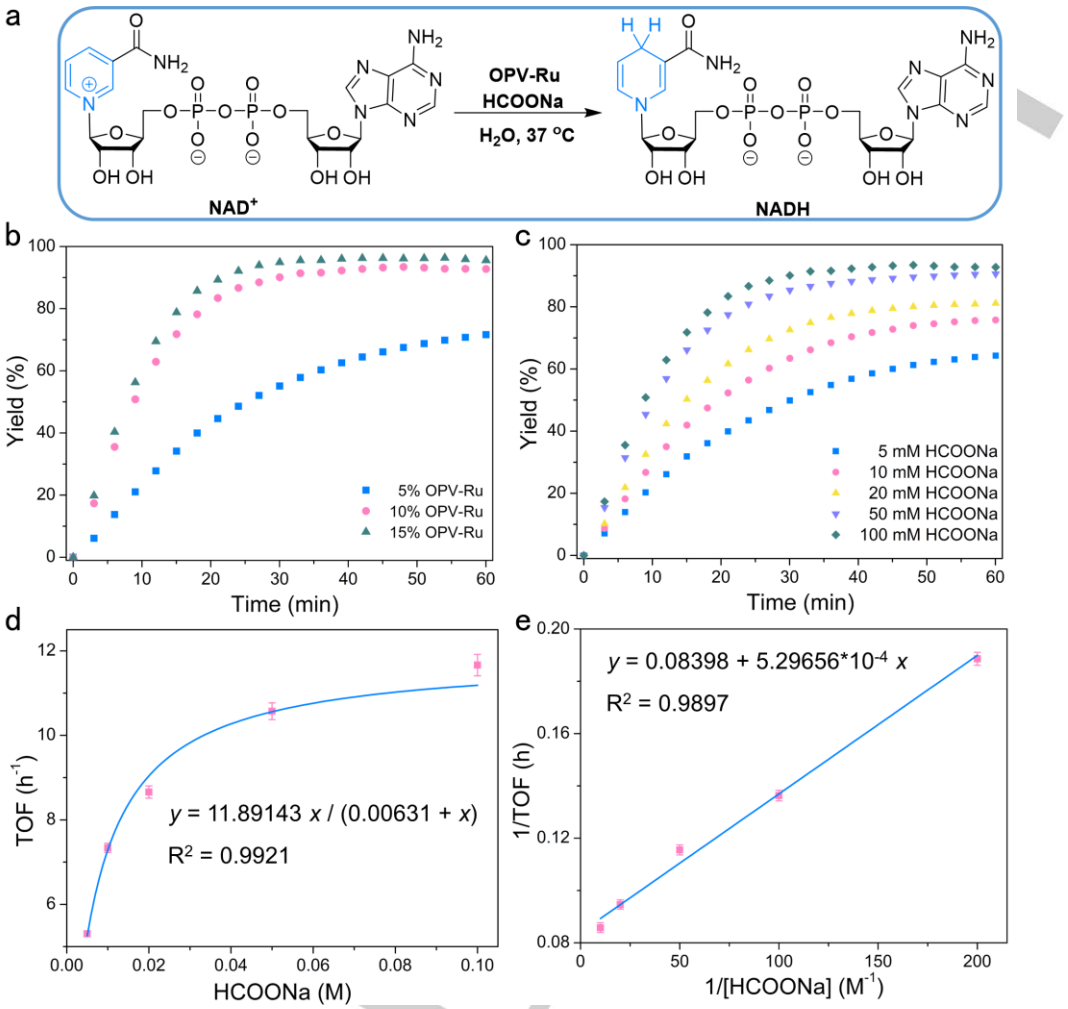

Figure 3. a) Transfer hydrogenation of NAD^+ to NADH catalyzed by OPV-Ru with HCOONa as hydrogen source. b) Influence of OPV-Ru content on the conversion of NAD^+, [NAD^+] = 0.1 mM, [HCOONa] = 100 mM, in water, 37 °C. c) Effect of HCOONa concentration on the conversion of NAD^+, [NAD^+] = 0.1 mM, [OPV-Ru] = 0.01 mM, in water, 37 °C. d) Plot of the TOF against HCOONa concentration with a fitted Michaelis-Menten-type equation. e) Plot of the reciprocal of the TOF against HCOONa concentration.

formed extensive aggregates. With increasing the ratio of d_6-DMSO, the broad peaks gradually sharpened and were shifted downfield. For example, the signal of α proton was shifted from δ = 7.714 to 7.907 ppm over the ratio of DMSO increasing from 50% to 100% (**Fig. 2d**). Solvent-dependent ^{1}H NMR spectroscopy further revealed that OPV-Ru aggregated in water (**Fig. 2e**). Therefore, the self-assembly of OPV-Ru in water was verified clearly. It is noted that, in comparison with OPV-Ru, Ts-Ru lacks self-assembly capability as shown by its TEM, although it exhibits a larger hydration particle size (164.4 ± 5.3 nm) while with much smaller zeta potential (+3.63 ± 0.4 mV) (**Fig. S1**).

The catalytic activity of OPV-Ru in transforming NAD^+ to NADH with HCOONa as hydrogen source (**Fig. 3a**) in water was firstly assessed by UV-visible spectroscopy. The catalysis process was monitored with absorbance variation at 340 nm assigned to NADH over NAD^+. According to the standard curve of NADH concentration versus its absorbance at 340 nm (**Fig. S2**), the yield of NADH could be determined. Firstly, the effect of OPV-Ru concentration on this reaction was investigated with a fixed concentration of HCOONa (**Fig. 3b**). With 5% OPV-Ru, the NADH production yield reached 70% within 60 min. Upon increasing OPV-Ru to 10%, more NADH was produced with faster rate, reaching a yield of 93% within 45 min. Further increment of OPV-Ru to 15% nearly completed the transformation, giving a yield of 96% at 41 min. As HCOONa served as a hydrogen source, the effect of HCOONa concentration on this reaction was also studied (**Fig. 3c**). With increasing concentration of HCOONa from 5 mM to 100 mM, both the production of NADH and reaction rate were improved, which shows that HCOONa could accelerate this catalytic process. Plot of the TOF versus HCOONa concentration indicated a typical Michaelis – Menten behavior (**Fig. 3d**). From the reciprocal of TOF versus HCOONa concentration, the maximum turnover frequency (TOF_{max}) and Michaelis constant (K_M) were determined to be 11.91 h^{-1} and 6.3 mM, respectively (**Fig. 3e**).

To investigate the relationship between aggregation of OPV-Ru and its catalytic efficiency, we compared OPV-Ru and catalysis center (*p*-cymene)Ru(TsEn)Cl (Ts-Ru, **Fig. 4a**) on the

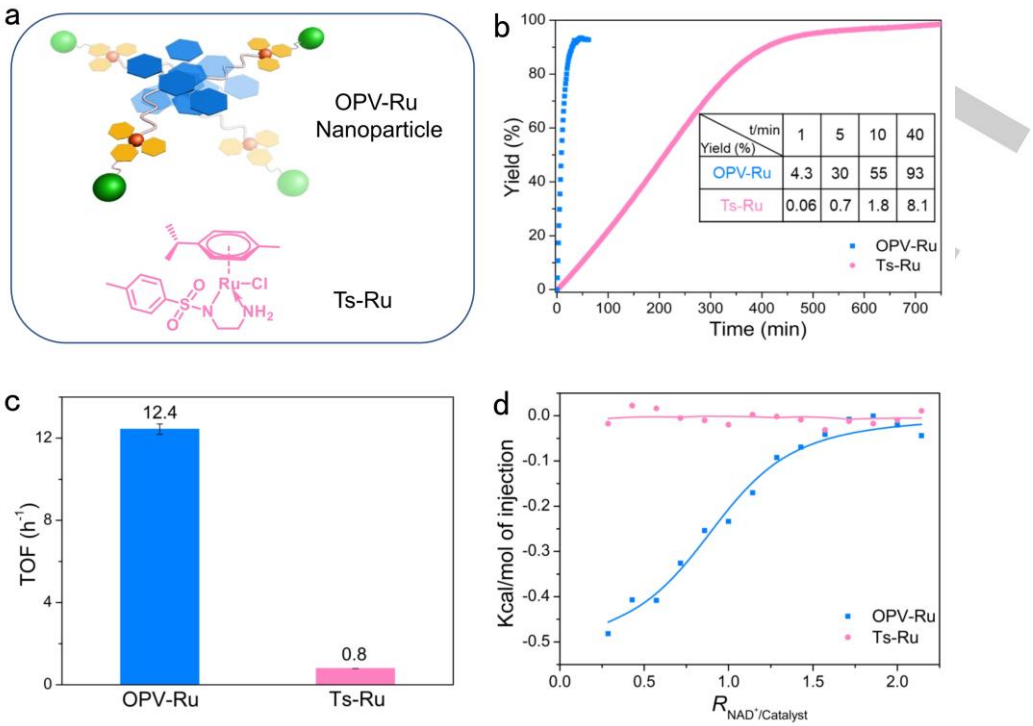

Figure 4 a) Chemical structures of OPV-Ru aggregate and dispersed Ts-Ru. b) Transfer hydrogenation of NAD^+ by OPV-Ru and Ts-Ru in water at 37 °C. [NAD^+] = 0.1 mM, [OPV-Ru] = 0.01 mM, [Ts-Ru] = 0.01 mM, [HCOONa] = 100 mM. c) TOF values of OPV-Ru and Ts-Ru. d) ITC result, where observed enthalpy changes against NAD^+/catalyst ratio by titrating 5 mM NAD^+ into 0.2 mM OPV-Ru or Ts-Ru in water.

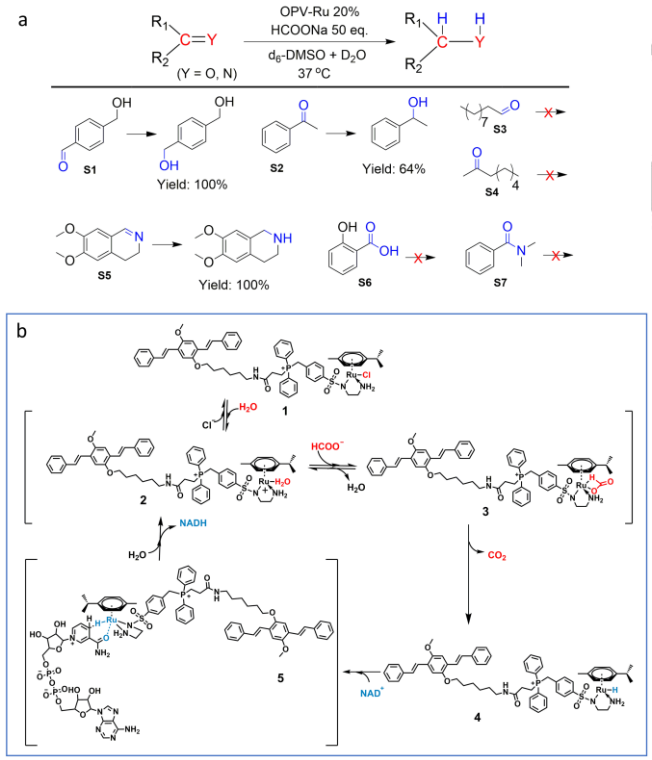

Figure 5. a) Scope of the OPV-Ru catalyzed transfer hydrogenation. [Substrate] = 2 mM, [OPV-Ru] = 0.4 mM, [HCOONa] = 50 mM, in D_2O and d_6-DMSO (3:2), 37 °C. ^1H NMR was employed to monitor the reaction and determine the yield. b) Proposed mechanism for OPV-Ru catalyzed reduction of NAD^+ in water with HCOONa as hydrogen source.

transfer hydrogenation of NAD^+, as Ts-Ru lacks self-assembly capability (shown in **Fig. S1)**. As shown in **Fig. 4b**, the transfer hydrogenation catalyzed by OPV-Ru reached endpoint at about 45 min while Ts-Ru required more than 600 min under the same condition. It is remarkable that OPV-Ru realized 55% yield within 10 min while Ts-Ru only reached a yield of 1.8%, which clearly revealed the high catalytic efficiency of OPV-Ru. In addition, calculated TOF value of OPV-Ru was 14.5 folds higher than that of Ts-Ru (**Fig. 4c**). Since both OPV-Ru and Ts-Ru are positively charged with a zeta potential of +23.1 ± 0.8 mV and +3.63 ± 0.4 mV, respectively, while NAD^+ is negatively charged, we utilized isothermal titration calorimetry (ITC) to verify the relationship of catalyst activity and their interactions with NAD^+. As shown in **Fig. 4d**, the ITC results demonstrated that the interaction between OPV-Ru and NAD^+ was an exothermic process, and its binding constant was measured to be 7.04 x 10^4 M^{-1} with a binding ratio of 0.896. However, there was no obvious enthalpy change in the titrating process of NAD^+ to Ts-Ru. These results showed that NAD^+ preferred to bind to OPV-Ru nanoparticles rather than dispersed Ts-Ru. Thus, OPV-Ru nanoparticles with dense positive charges can bring substrates and catalytic centers into closer proximity and provide a local microenvironment for significantly enhancing the catalytic efficiency.

Different types of substrate, including aldehyde, ketone, imine, carboxylic acid and amide, were employed for the transfer hydrogenation catalyzed by OPV-Ru, with HCOONa as hydrogen source in D_2O/d_6-DMSO (v/v = 3 : 2) at 37 °C (**Fig. 5a**). These reactions were all confirmed by ^1H NMR spectra (**Fig. S3**). OPV-Ru displayed a good activity in the reduction of C=O of aromatic aldehyde S1 and C=N of aromatic imine S5 both with 100% yield, moderate activity in transforming C=O of aromatic

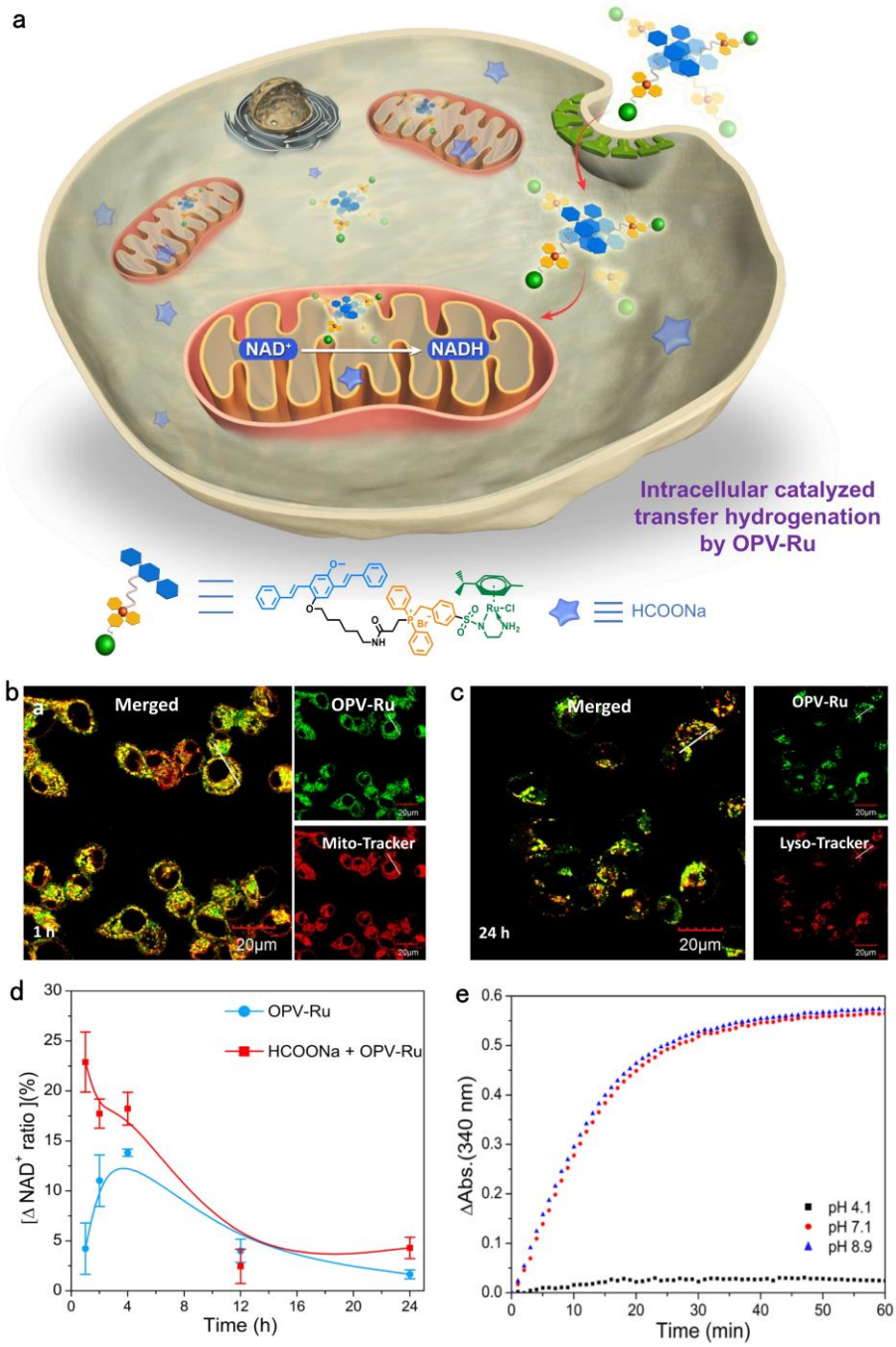

Figure 6. a) Intracellular transfer hydrogenation of NAD^+ to NADH catalyzed by OPV-Ru with HCOONa as hydrogen source. b) Mitochondria targeting ability of OPV-Ru and its dynamic distribution in living cells. Colocalization of OPV-Ru and Mito-Tracker Red-FM dye in A2780 cells after incubation for 1 h. c) Colocalization of OPV-Ru and Lyso-Tracker DND 99 in A2780 cells after incubation for 24 hours. d) Intracellular NAD^+ ratio variation after treatment of A2780 cells with fresh medium, HCOONa (2 mM), OPV-Ru (16 μM) and HCOONa (2 mM) + OPV-Ru (16 μM) for 1 h, 2 h, 4 h, 12 h and 24 h, respectively. NAD^+ ratio = $[NAD^+]/[\text{total } NAD^+/NADH]$. For blue line: Δ NAD^+ ratio = (NAD^+ ratio in blank group) - (NAD^+ ratio in OPV-Ru group); for red line: Δ NAD^+ ratio = (NAD^+ ratio in HCOONa group) - (NAD^+ ratio in HCOONa + OPV-Ru group). e) Influence of pH on the conversion of NAD^+ at 37 °C. $[NAD^+]$ = 0.1 mM, [HCOONa] = 100 mM, [OPV-Ru] = 0.01 mM.

ketone S2 with 64% yield, while no reactions were observed for alkyl aldehyde S3, alkyl ketone S4, aromatic carboxylic acid S6 and aromatic amide S7. The chemoselectivity of OPV-Ru indicated its good biocompatibility as biological systems are mostly composed of amino acids and proteins. Based on previous research on Noyori-type ruthenium catalysts, a possible mechanism for the transfer hydrogenation of NAD^+ by OPV-Ru was proposed (**Fig. 5b**). It mainly involved interactions between OPV-Ru (1) and H_2O and HCOONa via intermediates 2 and 3 to generate active species OPV-Ru-H (4). This active intermediate reacted with NAD^+ to form a hexatomic ring species (5) following by the generation of NADH and the catalyst returned to its original state. It is apparent that interaction between OPV-Ru and substrate NAD^+ is vital for the whole catalytic process.

After a series of characterization in aqueous solution, OPV-Ru was introduced into living cells for biological application (**Fig. 6a**). We first investigated its ability in targeting mitochondria and A2780 human ovarian cancer cell was selected as a representative. MTT assay (**Fig. S4**) showed that OPV-Ru lower than 16 μM had little effect on the growth of A2780 cells, which verified a good biocompatibility of OPV-Ru. OPV-Ru could enter A2780 cells within 1 hour and was mostly located in mitochondria with a Pearson correlation coefficient of 0.85, demonstrated by colocalizing OPV-Ru with the mitochondrion tracker dye (**Fig. 6b**). After continuous incubation for 12 hours, most OPV-Ru remained accumulated in mitochondria with a Pearson correlation coefficient of 0.74 (**Fig. S5a**-**b**). Whereas after incubation of 24 hours, the confocal images showed that almost no OPV-Ru existed in mitochondria (**Fig. S5c-d**). Further colocalization with lysosomal tracker dye demonstrated its wide distribution in lysosomes (**Fig. 6c**). Through cell imaging, the mitochondria targeting ability of OPV-Ru and its dynamic distribution in cells were clearly revealed. To deeply investigate the endocytosis mechanism of OPV-Ru, A2780 cells were treated in different conditions including low temperature (4 ºC), dynasore, chlorpromazine (CPZ), sucrose and nystatin. Then cells were photographed using confocal laser scanning microscopy (CLSM) (**Fig. S6a**) and fluorescence intensity of OPV-Ru in each image were analyzed quantitatively (**Fig. S6b**). It was observed that the internalization of OPV-Ru was strongly inhibited at 4 ºC, which implied the endocytosis process was energy-dependent. In addition, the uptake was completely suppressed by dynasore, an inhibitor of dynamin, which is essential for clathrin-dependent coated vesicle formation as well as some clathrin-independent endocytosis pathways such as caveolae-dependent pathway. However, the endocytosis was scarcely suppressed by nystatin, which excluded a caveolae-dependent endocytosis pathway. In addition, the fluorescence of OPV-Ru was decreased to 19% and 59% in the presence of sucrose and CPZ, respectively. Therefore, the internalization was mostly dominated by clathrin-dependent endocytosis pathway.

The catalytic activity of OPV-Ru in cells was investigated through NAD^+/NADH ratio assay kit, which can measure the content of total NAD^+/NADH as well as NAD^+. Initially, cytotoxicity of HCOONa was evaluated by MTT assay (**Fig. S4b**), which showed that millimolar level of HCOONa was nontoxic to cell growth. Four groups were set up for comparison, including blank group, group treated with HCOONa, group treated with OPV-Ru and group treated with HCOONa/OPV-Ru. After incubation for 1, 2, 4, 12 and 24 hours, respectively, cells of the four groups were respectively collected and treated for measurement. At 1 hour, NAD^+ ratio in blank group was found to be 71% and OPV-Ru alone barely affected NAD^+ ratio of cells. While HCOONa/OPV-Ru decreased the ratio of NAD^+ by 23%, compared with that in HCOONa group (**Fig. S7a**). The results demonstrated a high catalytic activity of OPV-Ru in converting NAD^+ to NADH intracellularly. After 2 hours, in comparison with HCOONa group, NAD^+ ratio in group of HCOONa/OPV-Ru was reduced by 18% (**Fig. S7b**). It is worth mentioning that NAD^+ ratio in OPV-Ru group was decreased by 11%, compared to that of blank group. It is different from the transfer hydrogenation in aqueous solution, which requires both OPV-Ru and HCOONa. Probably endogenous reductants served as hydrogen source here. Similarly, after 4 hours, intracellular NAD^+ ratios in the presence of OPV-Ru and HCOONa/OPV-Ru were both decreased by certain proportion (**Fig. S7c**). After 12 hours, almost no change of NAD^+ ratio could be monitored in the experimental groups, compared to that of blank group (**Fig. S7d**), which implied that intracellular NAD^+ and NADH reached a state of balance again. The comparison for OPV-Ru group and blank group as well as that for HCOONa group and HCOONa/OPV-Ru group are summarized (**Fig. 6d**), from which conditions and rules of intracellular catalysis by OPV-Ru were clearly figured out. It is noted that, 24 hours later, also no obvious NAD^+ ratio variation in experimental groups was detected (**Fig. S7e**), which probably because this catalysis cannot proceed in lysosome. This is confirmed by the pH-dependent catalysis behavior of OPV-Ru. As shown in **Fig. 6e**, the reduction process cannot occur at pH 4.1, which it is apparent that OPV-Ru cannot play its catalytic role in lysosome, where environment is acidic.

In summary, we designed and synthesized a novel amphiphilic conjugated oligomer-based Noyori-type ruthenium complex OPV-Ru, which could self-assemble into nanoparticles in water. With numerous positive charges accumulated on the surface of OPV-Ru nanoparticles, it displayed a strong electrostatic interaction with negatively charged NAD^+ molecules, creating a local microenvironment for enhancing the catalytic transfer hydrogenation of NAD^+ to NADH. Benefiting from inherent fluorescence of OPV-Ru, the dynamic distribution in cells and uptake behavior of OPV-Ru could be traced under fluorescence microscopy. With a cationic benzyldiphenylphosphine group, OPV-Ru could selectively accumulate in mitochondria of living cells. Importantly, OPV-Ru displayed a remarkable activity in reducing intracellular NAD^+ ratio. Overall, this work provides a new strategy for designing multifunctional organometallic complex to work perfectly inside living cells with excellent performance, including fluorescent imaging ability, specific mitochondria targeting, good chemoselectivity and high catalysis efficiency.

Acknowledgements

The authors are grateful to the National Natural Science Foundation of China (Nos. 21533012, 21661132006) and the Strategic Priority Research Program of the Chinese Academy of Sciences (XDA16020804).

Keywords: ruthenium catalyst • biocatalysis • intracellular catalysis • transfer hydrogenation • mitochondria

[1] Bai, Y., Chen, J., Zimmerman, S. C. *Chem. Soc. Rev.* 2018, 47, 1811-1821.
[2] Soldevila-Barreda, J. J., Metzler-Nolte, N. *Chem Rev.* 2019, 119, 829-869.
[3] Ngo, A. H., Bose, S., Do, L. H. *Chem. Eur J.* 2018, 24, 10584-10594.
[4] Jeschek, M., Reuter, R., Heinisch, T., Trindler, C., Klehr, J., Panke, S. & Ward, T. R. *Nature* 2016, 537, 661-665.
[5] Liu, Z., Romero‐Canelón, I., Qamar, B., Hearn, J. M., Habtemariam, A., Barry, N. P., Sadler, P. J. *Angew. Chem. Int. Ed.* 2014, 53, 3941-3946.
[6] Clavadetscher, J., Indrigo, E., Chankeshwara, S. V., Lilienkampf, A., Bradley, M. *Angew. Chem. Int. Ed.* 2017, 129, 6968-6972.
[7] Yusop, R. M., Unciti-Broceta, A., Johansson, E. M., Sánchez-Martín, R. M., Bradley, M. *Nat. Chem*. 2011, 3, 239-243.
[8] Bai, Y., Feng, X., Xing, H., Xu, Y., Kim, B. K., Baig, N., Zimmerman, S. C. *J. Am. Chem. Soc.* 2016, 138, 11077-11080.

[9] Tonga, G. Y., Jeong, Y., Duncan, B., Mizuhara, T., Mout, R., Das, R., Rotello, V. M. *Nat. Chem.* 2015, 7, 597-603.
[10] Miller, M. A., Askevold, B., Mikula, H., Kohler, R. H., Pirovich, D., Weissleder, R. *Nat. Commun*. 2017, 8, 15906-15918.
[11] Clavadetscher, J., Indrigo, E., Chankeshwara, S. V., Lilienkampf, A., Bradley, M. *Angew. Chem. Int. Ed*. 2017, 129, 6968-6972.
[12] Coverdale, J. P., Romero-Canelón, I., Sanchez-Cano, C., Clarkson, G. J., Habtemariam, A., Wills, M., Sadler, P. J. *Nat. Chem.* 2018, 10, 347-354.
[13] Tomás-Gamasa, M., Martínez-Calvo, M., Couceiro, J. R., Mascareñas, J. L. *Nat. Commumn*. 2016, 7, 12538-12547.
[14] Zhou, L., Lv, F., Liu, L., Shen, G., Yan, X., Bazan, G. C., Wang, S. *Adv. Mat.* 2018, 30, 1704888-1704895.
[15] Chen, Y., Zhou, L., Wang, J., Liu, X., Lu, H., Liu, L., Wang, S. *ACS Appl. Mater. Interfaces* 2018, 10, 27555-27561.
[16] Li, M., He, P., Li, S., Wang, X., Liu, L., Lv, F., Wang, S. *ACS Biomater. Sci. Eng*. 2017, 4, 2037-2045.
[17] Yamakawa, M., Ito, H., Noyori, R. *J. Am. Chem. Soc.* 2000, 122, 1466-1478.
[18] Wang, D., Astruc, D. *Chem Rev.* 2015, 115, 6621-6686.
[19] Matsunami, A., Kayaki, Y. *Tetrahedron Lett.* 2018, 59, 504-513.
[20] Zielonka, J., Joseph, J., Sikora, A., Hardy, M., Ouari, O., Vasquez-Vivar, J., Kalyanaraman, B. *Chem. Rev.* 2017, 117, 10043-10120.
[21] Verdin, E. *Science* 2015, 350, 1208-1213.
[22] Chiarugi, A., Dölle, C., Felici, R., Ziegler, M. *Nat. Rev. Cancer*. 2012, 12, 741-752.
[23] Ying, W. *Front Biosci*. 2006, 11, 3129-3148.
[24] Zhao, Y., Wang, A., Zou, Y., Su, N., Loscalzo, J., Yang, Y. *Nat. Protocols*. 2016, 11, 1345-1359.
[25] Zhu, X. H., Lu, M., Lee, B. Y., Ugurbil, K., Chen, W. *Proc. Natl. Acad. Sci. USA* 2015, 112, 2876-2881.

10.1002/chem.201905448

WILEY-VCH

A multifunctional metal catalyst, ruthenium-coordinated oligo(*p*-phenylenevinylene) (OPV-Ru) is developed for intracellular catalysis of transfer hydrogenation reaction. OPV-Ru self-assembles into nanoparticles and subsequently work perfectly inside living cells with excellent performance, including fluorescent imaging ability, specific mitochondria targeting, good chemoselectivity and high catalysis efficiency.

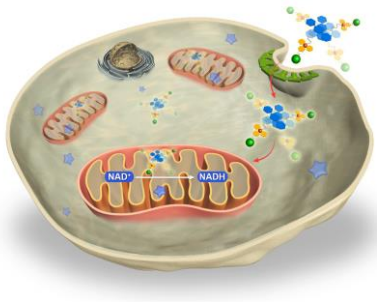

Nan Dai, Hao Zhao, Ruilian Qi, Yanyan Chen, Fengting Lv, Libing Liu and Shu Wang

Page No. – Page No.

Fluorescent and Biocompatible Ruthenium-Coordinated Oligo(*p*-phenylenevinylene) Nanocatalyst for Transfer Hydrogenation in Mitochondria of Living Cells